



## FABRICATION AND CHARACTERIZATION OF $\text{Al}_2\text{O}_3$ - $\text{CeO}_2$ COATING ON TA6V SUBSTRATE FOR HIGH TEMPERATURE APPLICATIONS

S. GUERFI<sup>a</sup>, S. HAMDI<sup>b</sup>, E. B. HANNECH<sup>a\*</sup> and M. BOUODINA<sup>c,d</sup>

<sup>a</sup>LESIMS, Badji Mokhtar Annaba University, 23000, ALGERIA

<sup>b</sup>Chadli Bendjedid El Tarf University, 36000, ALGERIA

<sup>c</sup>Department of Physics, College of Science, University of Bahrain, PO Box 32038, BAHRAIN

<sup>d</sup>Nanotechnology Centre, University of Bahrain, PO Box 32038, BAHRAIN

### ABSTRACT

Al and Ce films have been deposited on TA6V alloy by physical vapor deposition of Al and cathodic electrode position process from a  $\text{Ce}(\text{NO}_3)_3$ ,  $6\text{H}_2\text{O}$  and mixed water-ethyl alcohol solution at 0.01 M, respectively. The experimental conditions for the achievement of a uniform deposit, adherent and non-cracking were identified and determined by electrochemical methods. The transformation of the deposited layers into  $\text{CeO}_2$  and  $\text{Al}_2\text{O}_3$  oxides obtained by heat treatment of the coated alloy, is expected to increase the resistance to high temperature oxidation. The coating films were characterized by differential scanning calorimetry (DSC), X-ray diffraction (XRD) and scanning electron microscopy (SEM).

**Key words:** Titanium alloy, Cerium oxide, Aluminum, Electrodeposition, Coatings.

### INTRODUCTION

Titanium-based alloys possess good corrosion resistance and creep for temperatures below  $500^\circ\text{C}$ . However, at higher temperatures, the resistance to oxidation decreases rapidly caused by the formation of  $\text{TiO}_2$  at the surface. The addition of rare earth elements such as Ce, Y, Er, La to the alloy improved its corrosion resistance. Rare earth (RE) oxide thin films exhibiting important physical, chemical and thermal properties that are of great interest for numerous industries in particular in protective coatings at different systems, including metallic coatings<sup>1</sup>, nitride coatings<sup>2</sup>, diffusion coatings<sup>3</sup> and ceramic coatings<sup>4</sup>. Therefore, RE oxides are extensively applied on Ti-based alloys. However, the disadvantages associated with the adhesion brittleness of the coatings are reasonable and it is necessary to develop techniques and coating systems in order to improve the oxidation resistance of Ti-based alloys.

---

\* Author for correspondence; E-mail: eb\_hannech@yahoo.fr; Ph.: +213773431945

In recent years, several studies have shown that surface treatment by using coatings has considerably improved wear, corrosion and oxidation resistances of Ti-based alloys. Different methods have been adopted for surface coatings such as MOCVD<sup>5</sup>, plasma<sup>6</sup>, dip coating<sup>7</sup>, and laser cladding<sup>8-10</sup>. In particular, electro-deposition has a wide range of applications in the processing of advanced ceramic materials and coatings.

Moreover, numerous research works have shown that  $Y_2O_3$ <sup>11</sup> and  $Al_2O_3$ - $Y_2O_3$  composite coatings were very compact and consisted of uniform nanoparticles<sup>12</sup> resulting in significant improvement of the oxidation of  $\gamma$ -TiAl alloy<sup>13</sup>.  $TiAl_3$  phase is rich enough in Al to promote the formation of a covering, compact and protective alumina layer<sup>14</sup>. The corrosion resistance of MOCVD  $Al_2O_3$  coating on TA6V alloy has been investigated<sup>5</sup>; the coating showed the lowest salt damage on Ti substrate compared to uncoated while exhibited a good adherence. It has been shown that amorphous alumina coating improves TA6V corrosion resistance at 700°C in comparison with others oxide films<sup>15</sup>. The adhesion between the coating layer and the base of substrate is necessary and can be obtained through the formation of an intermediate region; i.e. coating-substrate interface<sup>16</sup>. The surface of a duplex treated TA6V (laser nitride and PVD TiN coated) has more resistance to corrosion in comparison to TiN coated and untreated surfaces<sup>8</sup>. The PVD coating is widely used in fatigue, wear and corrosion protection of TA6V<sup>17</sup>.

In the present study, double coatings of TA6V alloy is performed in two steps; thin Al layer by PVD followed by Ce layer by electrodeposition method. Subsequent thermal treatment is performed in order to form  $CeO_2$ . The as-obtained Ti sample with double coatings is subjected to high temperature oxidation.

## EXPERIMENTAL

### Sample preparation

A Ti alloy rod (Ti-wt. 90%, Al-wt.6%, V-wt.4%) with a 10 mm diameter was cut into 2 mm thickness coupons. Near the edge of each coupon, a 1.5 mm diameter hole was drilled for sample suspension.

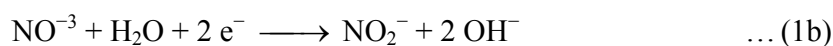
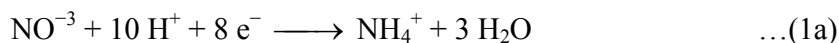
Just before the electrodeposition of the films, the substrates (the coupons) were mechanically polished with emery papers and 1  $\mu$ m diamond paste, ultrasonically cleaned in an acetone bath, rinsed with distilled water and dried with hot air. After that, a thin layer (around 1  $\mu$ m thick) of Al was deposited by PVD (Joule effect) technique onto TA6V substrate. The evaporation was performed in a chamber under a vacuum of  $10^{-6}$  torr.

## Films deposition and process

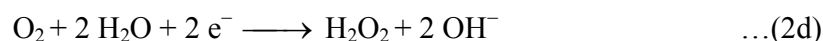
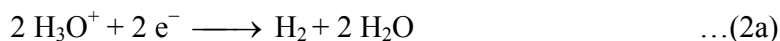
A 0.01 M solution obtained by dissolution of cerium nitrate  $\text{Ce}(\text{NO}_3)_3$  in water-ethyl alcohol, was used for oxide films electrodeposition. The electrodeposition experiment was performed using a three electrode cell; the substrate as cathode, a platinum grid as counter electrode and the reference a saturated calomel electrode (SCE). The film deposition was performed in galvanostatic mode without stirring the solution at a scan rate of 20 mV/s, at room temperature. After electrodeposition, the samples were rinsed with ethyl alcohol and air dried for at least an overnight before<sup>18</sup>.

The electrochemical mechanism of base electro-generation during cathodic deposition has been widely discussed in the literature<sup>19-23</sup> in the case of nitrate baths, where the anion participates in the cathodic reaction. Several chemical reactions can occur during film electrodeposition according to some previous research works<sup>19-21,24-28</sup>:

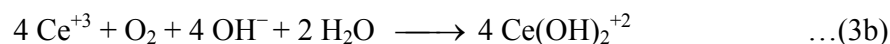
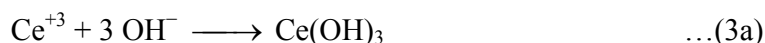
### Nitrate reduction



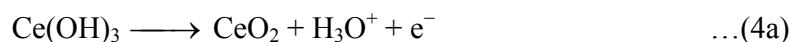
### $\text{O}_2$ , $\text{H}_2\text{O}$ , $\text{H}_3\text{O}^{+}$ reduction



### Formation of $\text{Ce}(\text{OH})_3$ and/or $\text{Ce}(\text{OH})_2^{+2}$



### Oxidation of $\text{Ce}^{+3}$ to $\text{Ce}^{+4}$



## Characterization

The microstructure of the deposited films was studied by scanning electron microscopy (SEM) using Tescan Vega 3 Lmu coupled to an X-ray energy dispersive spectrometer (EDS). The crystal structure was characterized by X-ray diffraction (XRD) using Bruker AXS D8-Advance diffractometer equipped with Cu radiation source (wavelength  $\lambda_{\text{Cu}} = 0.15406$  nm) at a scan rate of  $0.04^\circ/\text{s}$ . Differential scanning calorimetry (DSC) measurements were carried out using DSC 131 Setaramin argon atmosphere in the range  $40\text{-}560^\circ\text{C}$  at a heating rate of  $10^\circ\text{C}/\text{min}$  and then cooled down to room temperature.

## RESULTS AND DISCUSSION

### Polarization experiments

Cathodic polarization curves for TA6V at room temperature are shown in Fig. 1; these curves were obtained in a mixed water-ethanol solution of cerium nitrate, without stirring. The polarization curves obtained can be divided in three main domains. In the first domain, for potential higher than  $-1.1$  V, low current densities are observed. This phenomenon is due to the reduction of dissolved oxygen with the nitrate according to Eq. (1)<sup>29</sup>. In the second domain ranging from  $-1.79$  to  $-1.1$  V/ECS, the cathodic current density increases rapidly due to water reduction to form  $\text{H}_2$  (Eq. 2) and hydrogen evolution reaction (HER). Finally, the change of slope appearing at  $-1.79$ ,  $-1.83$  and  $-2.1$  V/ECS was attributed to the adsorption of hydrogen bubbles, which blocked the electrode surface and to the reduction of  $\text{Ce}^{3+}$  ions (Eq. 3)<sup>30</sup>.

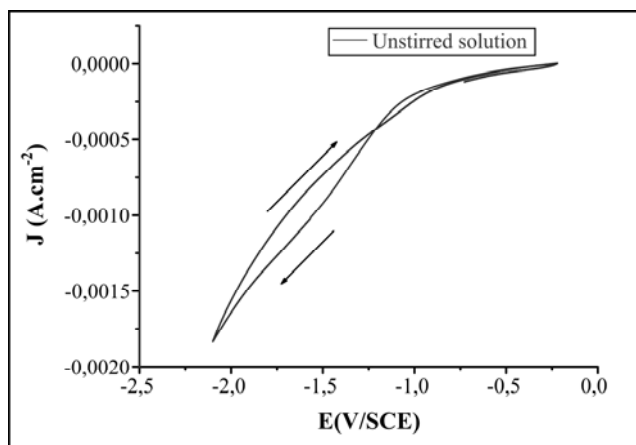


**Fig. 1: Cyclicvoltammograms performed on the uncoated TA6V from 0.01 M Ce nitrate solutions (Scanning rate: 20 mV/S)**

## Galvanostatic deposition

Experiments carried out on galvanostatic mode, without stirring and with varying cathode current density, revealed that the evolution of the surface potential with the applied current density in bath depends on the mechanisms related to film' formation<sup>31</sup>. These mechanisms are related mostly to both oxygen and nitrates reduction reactions and some hydrogen evolution reaction (HER) for the short times and only to the HER for the longer times.

The effect of current density on film morphology has been investigated in order to obtain homogeneous and crack free thin films. For a current density of  $-1 \text{ mA.cm}^{-2}$ , the film formation is rapid and an important network of cracks appears in the coating and can be only observed in SEM image (see Fig. 2). To avoid the formation of cracks, smaller intensity values, ranging from  $-0.05$  to  $-0.2 \text{ mA.cm}^{-2}$  were then selected in order to lower the electrodeposition rate.

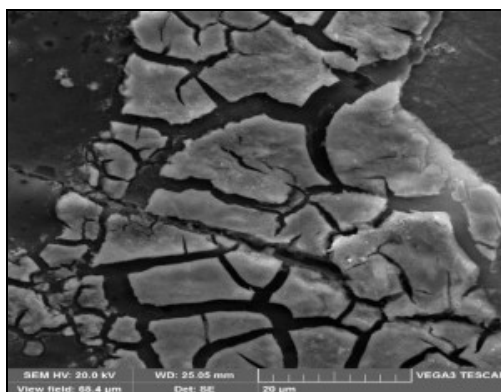


**Fig. 2: SEM micrograph of cerium alloy deposit ( $j = -1 \text{ mA.cm}^{-2}$ , deposition time 1800s), showing the cracking of the film**

Fig. 3 shows the evolution of the potential with time at different current densities for the  $0.1 \text{ M Ce(NO}_3)_3$  concentration during deposition. It can be seen that the electrochemical potential obtained at  $j = -0.05 \text{ mA.cm}^{-2}$  decreases slowly and monotonously up to 1500 s and then stabilizes at a cathodic value of about  $-0.26 \text{ V/SCE}$ . On the other hand, at current densities lower than  $j = -0.05 \text{ mA.cm}^{-2}$  ( $j = -0.1$  and  $j = -0.2 \text{ mA.cm}^{-2}$ ), it decreases rapidly in the first few seconds and then stabilize; the potential values are less cathodic than for higher current densities ( $j = -0.02 \text{ mA.cm}^{-2}$ ). The potential stabilization appears sooner, when decreasing the applied current density. The change of the shape of the polarization curves with the applied current densities can be related to the reduction reactions taking place at the

electrode, which may thus influence the morphology of the coatings<sup>31</sup>. A potential varying continuously with time indicates the occurrence of a single reaction, whereas sudden changes are indicative of a change in the dominant reaction taking place at the electrode<sup>32</sup>.

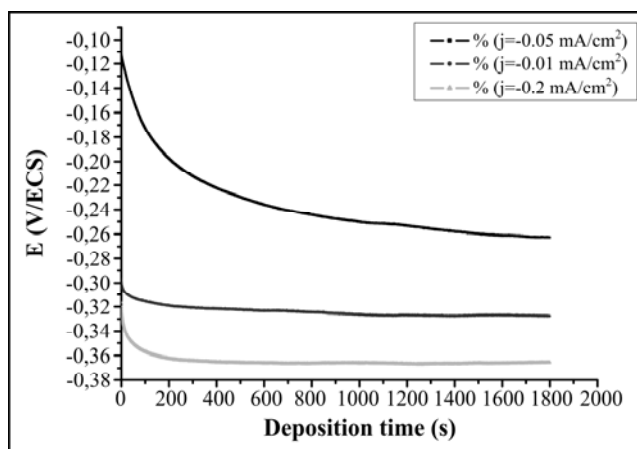


**Fig. 3: Variation of potential with time during cathodic deposition at  $j = -0,05 \text{ mA}\cdot\text{cm}^{-2}$ ,  $-0,01 \text{ mA}\cdot\text{cm}^{-2}$ ,  $-0,2 \text{ mA}\cdot\text{cm}^{-2}$**

A homogeneous film (Fig. 4) is obtained after a deposition time of 1800 s under  $j = -0,2 \text{ mA}\cdot\text{cm}^{-2}$ ; this current density has been chosen for further characterization.

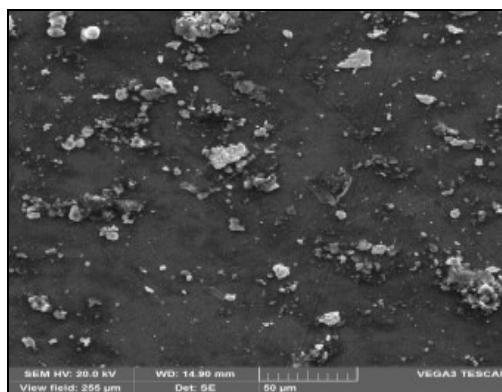


**Fig. 4: SEM micrograph of cerium alloy deposit ( $j = -0,2 \text{ mA}\cdot\text{cm}^{-2}$ )**

### Morphology of surface films

SEM micrographs of the film electrodeposited on TA6V at  $j = -0,2 \text{ mA}\cdot\text{cm}^{-2}$  for 900, 1800 and 3600 s are shown in Fig. 5. For 900 s, the treated sample surface contains some

cracks with the appearance of very thin and spherical grains (Fig. 5c). For 3600 s, the surface layer seems to be non-adherent (Fig. 5a). As discussed in literature, these cracks are associated with either the formation of gas bubbles; i.e. dehydration process<sup>31</sup> or constraints shear between the substrate and deposited layer<sup>32</sup>. For 1800 s, a very homogeneous film, adherent and without cracks completely covers TA6V surface. In addition to the random distribution of the crystals of the order of 10 microns over the entire sample surface (Fig. 5b), identified as grains of  $\text{Ce}(\text{OH})_3$ <sup>33,34</sup>, which is mainly composed by Ce, as was confirmed by EDX spectrum shown in Fig. 5d. According to the as-obtained results, a current density  $j = -0.2 \text{ mA}\cdot\text{cm}^{-2}$  with a deposition time of 1800 s were finally selected for further studies. As can be seen from the micrograph, the white localized spots were observed on the surface of conversion film, with Ce coating that was related to Ce hydroxide/hydrated oxide. Meanwhile, elemental chemical analysis indicated the existence of Ce in the coatings.

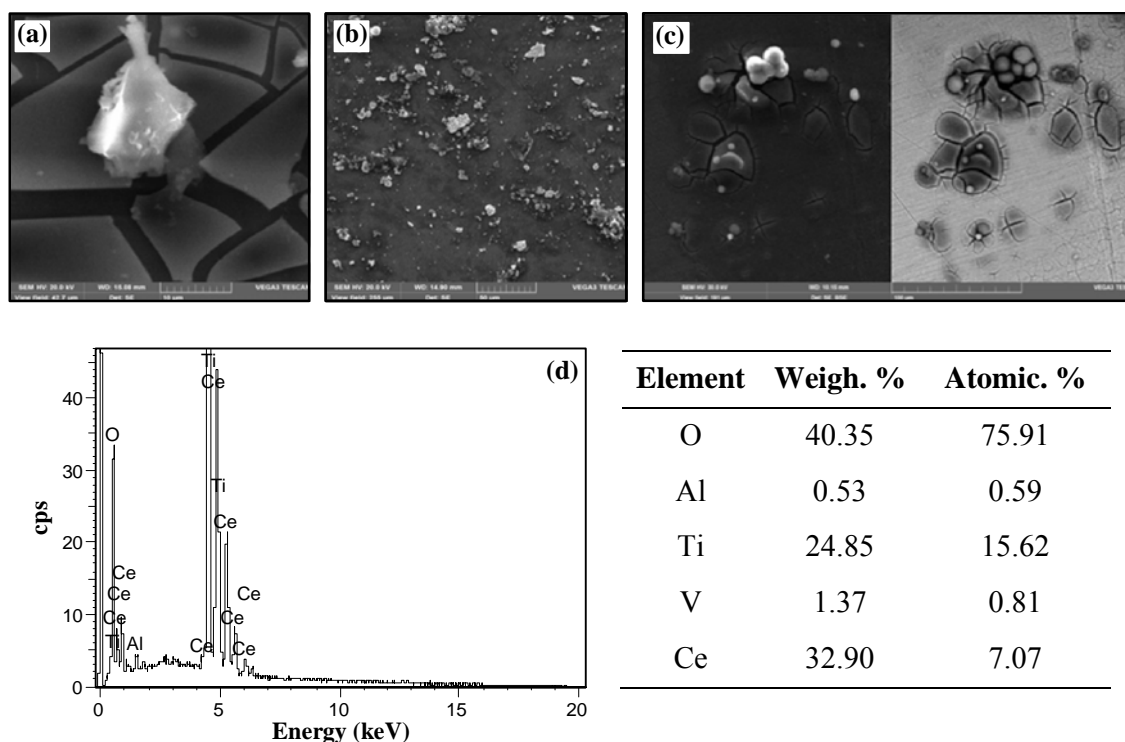


**Fig. 5: Evolution of SEM surface morphology of Ce oxide coating deposited from 0.01 M  $\text{Ce}(\text{NO}_3)_3$  with an applied current density  $j = -0.2 \text{ mA}\cdot\text{cm}^{-2}$  at different durations, (a) 3600 s, (b) 1800 s, (c) 900 s; (d) SEM-EDX Analysis for the coating prepared for ( $j = -0.2 \text{ mA}\cdot\text{cm}^{-2}$ ,  $t = 1800\text{s}$ ) showing the presence of Ce, Al, O and Ti**

### Effect of heat treatment

DSC measurement of  $\text{Ce}(\text{OH})_3$  powder was carried out between 50 and 550°C under pure argon flow and shown in Fig. 6. Two important steps during heating can be seen. First, the two exothermic peaks at ~169 and 243°C can be related to the release of free water and the crystallization of the amorphous portion hydroxide  $\text{Ce}(\text{OH})_3$  to crystalline oxide cerium  $\text{CeO}_2$ <sup>35-38</sup>, respectively. The second significant step concerns the endothermic peak at 500°C which is related to the conversion of hydroxide into cerium oxide (Eq. 4), and the formation of the fluorite (FCC) crystalline structure<sup>39,40</sup>. When a second cycle is performed on the same sample, three peaks are detected after cooling down to room temperature, which means that the product formed at the end of the first cycle is not stable.

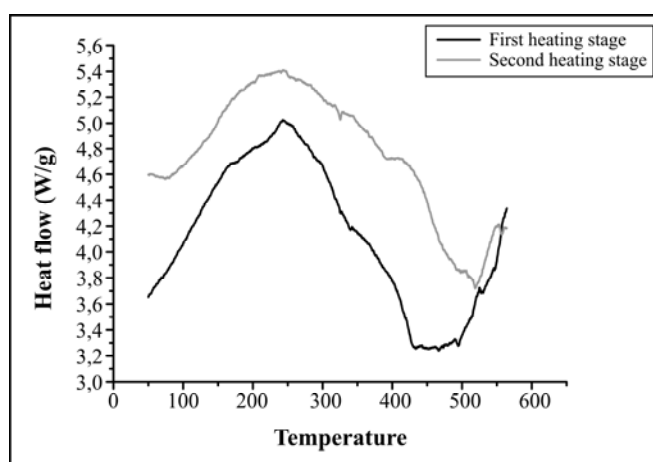


**Fig. 6: DSC analysis of the coating recorded in temperature range 40-560°C at 10°C.min<sup>-1</sup>**

### Phase composition analysis

X-ray diffraction patterns of as-prepared and heat treated (at 300 and 600°C for 1h under argon atmosphere) samples are shown in Fig. 7. The X-ray diffraction pattern of the samples that have been heat treated to 300°C presents speaks corresponding to one of the deposited dehydrations confirmed by DSC measurements; i.e. at 169 and 243°C. With increasing annealing temperature, the intensity of peaks increases indicating an improvement of the crystallinity of the coatings. At 600°C, the presence of composite coating oxide containing ( $\text{Al}_2\text{O}_3$ ) and ( $\text{CeO}_2$ ) can be evidenced, which was further confirmed with DSC analysis (peak at 500°C). This phase transition effectively leads to  $\text{CeO}_2$  and  $\text{Al}_2\text{O}_3$ , possibly by a new dehydration and decomposition of nitrate ions into nitrogen oxides, Eq. 3 (third

and fourth DSC peaks at 465 and 500°C). Thus, X-ray diffraction patterns of the sample heat treated at 300°C shows similar peaks but with higher intensity, which indicates that the DSC peak observed at 243°C corresponds to a dehydration coating. This result was also reported by Konstantinov et al.<sup>40</sup> during the deposition of CeO<sub>2</sub> on a fused silica substrate; Hamlaoui et al.<sup>36</sup> found two endothermic peaks at 130 and 145°C with DSC curves. Both have established that the heat treatment from 50 to 350°C has no effect on the morphology of the films of CeO<sub>2</sub>. The peak obtained by DSC at 500°C, describes the transformation of cerium hydroxides in crystalline oxide. This exothermic peak due to crystallization of CeO<sub>2</sub>, which is confirmed by the results of X-ray diffraction at 600°C and identified by Zitomirsky and Petric<sup>42,43</sup> and Sian et al.<sup>11</sup>. The sequence identified by Zitomirsky and Petric appears satisfactory to explain our exothermic peaks observed in our DSC analysis. This phase transition needs to be better identified; which is currently under progress.

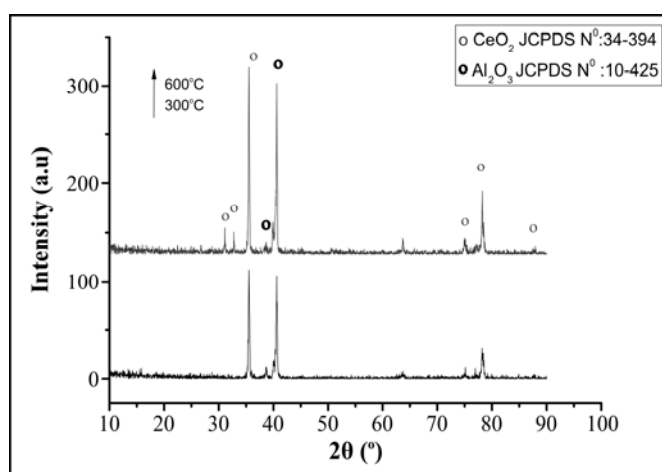


**Fig. 7: X-ray diffraction patterns of coated TA6V samples (deposition time 1800 s)**

## CONCLUSION

The aim of this study was to determine the optimum conditions to obtain, after heat treatment, thin layer of CeO<sub>2</sub>, suitable for high temperature corrosion for Ti-based alloy TA6V. It is found that this is highly dependent on the deposition parameters such as the applied current density, the deposition time and the composition of the bath. At high temperature, the reaction to produce hydrogen appears to prevent the formation of CeO<sub>2</sub> phase. At low densities, the oxide layer is found adherent, dense and has fine cracks. A homogeneous, uniform film of Ce (OH)<sub>2</sub> is obtained with a current density  $j = -0.2 \text{ mA}\cdot\text{cm}^{-2}$  and a time  $t = 1800 \text{ s}$ . Surface morphological observations obtained (SEM) show that the formed Ce(OH)<sub>2</sub> films are uniform and covered the entire surface. XRD analysis reveal that

the final coating is formed of CeO<sub>2</sub> with a cubic crystal structure (fluorite-type) and Al<sub>2</sub>O<sub>3</sub>. DSC analysis confirms the results obtained by XRD and describes the process of transformation of the hydroxide into oxide. The DSC results are in good agreement with the literature. The behavior of the treated samples seems to be promising and the combined Ce/Al oxides double coatings could be considered as an alternative for the high temperature Ti-based alloys protection.

### ACKNOWLEDGEMENT

The authors are thankful to D. Hamana (Mentouri University) for his contribution to DSC experiments, N. Benslim (Badji Mokhtar University) for his valuable help on PVD experiments, F. Djazi (Skikda University) for his contribution for SEM observations, B. Gasmi (Mohamed khider University) for his contribution for DRX analyses, and M. Daoudi and A. Triki (Badji Mokhtar University) for their help. The authors would also thank the Algerian Government for having funded this work.

### REFERENCES

1. Z. W. Li, W. Gao, Y. D. He, *Scr. Mater.*, **45**, 1099 (2001).
2. P. Eh. Hovsepain, A. P. Ehiasarian, R. Braun, J. Walker and H. Du, *Surf. Coat. Technol.*, **204**, 2702 (2010).
3. H. G. Jung, D. J. Jung and K. Y. Kim, *Surf. Coat. Technol.*, **154**, 75 (2002).
4. Z. L. Tang, F. H. Wang and W. T. Wu, *Mater. Sci. Eng.*, **A 276**, 70 (2000).
5. J. D. Beguin, D. Samelor, C. Vahlas, A. Gleizes, J. A. Petit and B. Sheldon, *Mater. Sci. Forum.*, **595**, 719 (2008).
6. A. L. Yerokhin, X. Nie, A. Leyland and A. Mat, *Surf. Coat. Technol.*, **21**, 195 (2000).
7. S. Y. Brou, R. Siab, G. Bonnet and J. L. Grosseau-Poussard, *Scripta Materialia.*, **56**, 517 (2007).
8. M. Khaled, B. S. Yilbas and J. Shirokoff, *Surf. Coat. Technol.*, **148-1**, 46 (2001).
9. Y. H. Lv, J. Li, Y. F. Tao and L. F. Hu, *Surf. Coat. Technol.*, **679**, 202 (2016).
10. F. Weng, H. Yu, C. Chen, J. Liu and L. Zhao, *J. Alloys Compd.*, **650**, 178 (2015).
11. R. Siab, G. Bonnet, J. M. Brossard, J. Balmain and J. F. Dinhut, *Appl. Surf. Sci.*, **253**, 3425 (2007).
12. J. Gao, Y. He and W. Gao, *Thin Solid Films*, **520**, 2060 (2012).

13. S. Hamdi, S. Guerfi and R. Siab, *Physics Procedia*, **2**, 737 (2009).
14. R. Gateau, Ph.D. Thesis, University of Bourgogne (2010).
15. D. Samélor, M. Aufray, L. Lacroix, Y. Balcaen, J. Alexis, H. Vergnes, D. Poquillon, J. D.Béguin, N. Pébère, S. Marcelin, B. Caussat and C. Vahlas, *Advan. Sci. Techno.*, **166**, 66 (2010).
16. B. S. Yilbas, M. S. J. Hashmi and S. Z. Shuja, *Surf. Coat. Technol.*, **140**, 244 (2001).
17. M. Y. P. Costa, M. L. R. Venditti, M. O. H. Cioffi, H. J. C. Voorwald, V. A. Guimarães and R. Ruas., **33**, 759 (2011).
18. J. M. Brossard, G. Bonnet, J. Balmain and J. Creus, *Surf. Coat. Technol.*, **185**, 275 (2004).
19. Y. Zhou and J. A. Switzer, *J. Alloys Compds.*, **237**, 1 (1996).
20. P. Stefanov, G. Atanasova, D. Stoychev and Ts. Marinova, *Surf. Coat. Technol.*, **180**, 446 (2004).
21. M. Balasubramaniana, C. A. Melendresa and A. N. Mansour, *Thin Solid Films*, **347**, 178 (1999).
22. L. Arurault, P. Monsang, J. Salley R. S. Bes, *Thin Solid Films*, **446**, 75 (2004).
23. J. Creus, F. Brezault, C. Rebere and M. Gadouleau, *Surf. Coat. Technol.*, **200**, 4636 (2006).
24. T. D. Golden and A. Q. Wang, *J. Electrochem. Soc.*, **150**, C621 (2003).
25. A. J. Aldykiewiczjr, A. J. Davenport and H. S. Isaacs, *J. Electrochem. Soc.*, **143**, 147 (1996).
26. F. B. Li, R. C. Newman and G. E. Tompson, *Electrochim. Acta*, **42**, 2455 (1997).
27. S. Kanakaraju, S. Mohan and A. K. Sood, *Thin Solid Films*, **305**, 191 (1997).
28. F. B. Li and G. E. Thompson, *J. Electrochem. Soc.*, **146**, 1809 (1999).
29. L. Gal-Or, I. Silberman, R. Chaim, *J. Electrochem. Soc.*, **138(7)**, 1939 (1991).
30. M. Pourbaix, *Atlas Electrochimique*, Gautiers-Villars & Cie Editeurs, Paris (1963).
31. Y. Hamlaoui, F. Pedraza, C. Remazeilles, S. Cohendoz, C. Rebere, L. Tifouti and J. Creus, *Mater. Chem. Phys.*, **113**, 650 (2009).
32. G. H. A. Therese and P. V. Kamath, *J. Appl. Electrochem.*, **28**, 539 (1998).

33. H. Y. Chang and H. I. Chen, *J. Cryst. Growth*, **283**, 457 (2005).
34. Y. Hamlaoui, L. Tifouti, C. Remazeilles and F. Pedraza, *Mater. Chem. Phys.*, **120**, 172 (2010).
35. J. Creus, F. Brezault, C. Rebere and M. Gadouleau, *Surf. Coat. Technol.*, **200**, 4636 (2006).
36. Y. Hamlaoui, F. Pedraza, C. Remazeilles, S. Cohendoz, C. Rebere, L. Tifouti and J. Creus, *Mater. Chem. Phys.*, **113**, 650 (2009).
37. N. Rane, H. Zou, Buelna and J. Y. S. Lin, *J. Member. Sci.*, **256**, 89 (2005).
38. B. N. Sivasankar, J. R. Sharmila, R. Saratha and S. Govindarajan, *Thermochim. Acta.*, **417**, 107 (2004).
39. R. C. Korosec, I. K. Skofic and N. Bukovec, *Thermochim. Acta*, **411**, 211 (2004).
40. K. Konstantinvo, I. Stambolova, P. Peshev, B. Darriet and S. Vassilev, *J. Inorg. Mat.*, **2**, 277 (2000).
41. I. Zhitomirsky and A. Petric, *Ceram. Int.*, **27**, 149 (2001).
42. I. Zhitomirsky and A. Petric, *Mater. Lett.*, **40**, 263 (1999).

*Revised : 27.10.2016*

*Accepted : 30.10.2016*